Received: 24 August 2020 | Revised: 27 October 2020 | Accepted: 30 October 2020

DOI: 10.1002/pro.3990

ARTICLE

THE PROTEIN SOCIETY WILEY

Frontotemporal dementia-linked P112H mutation of TDP-43 induces protein structural change and impairs its RNA binding function

Sashank Agrawal[1,2] | Monika Jain[1,2] | Wei-Zen Yang[1] | Hanna S. Yuan[1,2]

[1]Institute of Molecular Biology, Academia Sinica, Taipei, Taiwan

[2]Molecular and Cell Biology, Taiwan International Graduate Program, Academia Sinica and Graduate Institute of Life Sciences, National Defense Medical Center, Taipei, Taiwan

Correspondence
Hanna S. Yuan, Institute of Molecular Biology, Academia Sinica, Taipei 11529, Taiwan.
Email: hanna@sinica.edu.tw

Funding information
Ministry of Science and Technology, Taiwan; Academia Sinica

Abstract

TDP-43 forms the primary constituents of the cytoplasmic inclusions contributing to various neurodegenerative diseases, including amyotrophic lateral sclerosis and frontotemporal dementia (FTD). Over 60 TDP-43 mutations have been identified in patients suffering from these two diseases, but most variations are located in the protein's disordered C-terminal glycine-rich region. P112H mutation of TDP-43 has been uniquely linked to FTD, and is located in the first RNA recognition motif (RRM1). This mutation is thought to be pathogenic, but its impact on TDP-43 at the protein level remains unclear. Here, we compare the biochemical and biophysical properties of TDP-43 truncated proteins with or without P112H mutation. We show that P112H-mutated TDP-43 proteins exhibit higher thermal stability, impaired RNA-binding activity, and a reduced tendency to aggregate relative to wild-type proteins. Near-UV CD, 2D-nuclear-magnetic resonance, and intrinsic fluorescence spectrometry further reveal that the P112H mutation in RRM1 generates local conformational changes surrounding the mutational site that disrupt the stacking interactions of the W113 side chain with nucleic acids. Together, these results support the notion that P112H mutation of TDP-43 contributes to FTD through functional impairment of RNA metabolism and/or structural changes that curtail protein clearance.

KEYWORDS

neurodegenerative disease, protein aggregation, RNA recognition motif, RNA-binding protein

1 | INTRODUCTION

TDP-43 is a multifunctional protein that binds DNA and RNA, and it plays various roles in mRNA splicing, RNA transport, miRNA processing, and regulation of RNA stability and transcription.[1–3] TDP-43 contains an N-terminal domain (NTD) involved in protein dimerization,[4,5] two tandem RNA recognition motifs (RRM1 and RRM2) responsible for RNA binding, and an intrinsically disordered C-terminal glycine-rich region (G-rich) that exhibits prion-like properties involved in protein–protein interactions and aggregation (Figure 1a).[6–12] Cytoplasmic

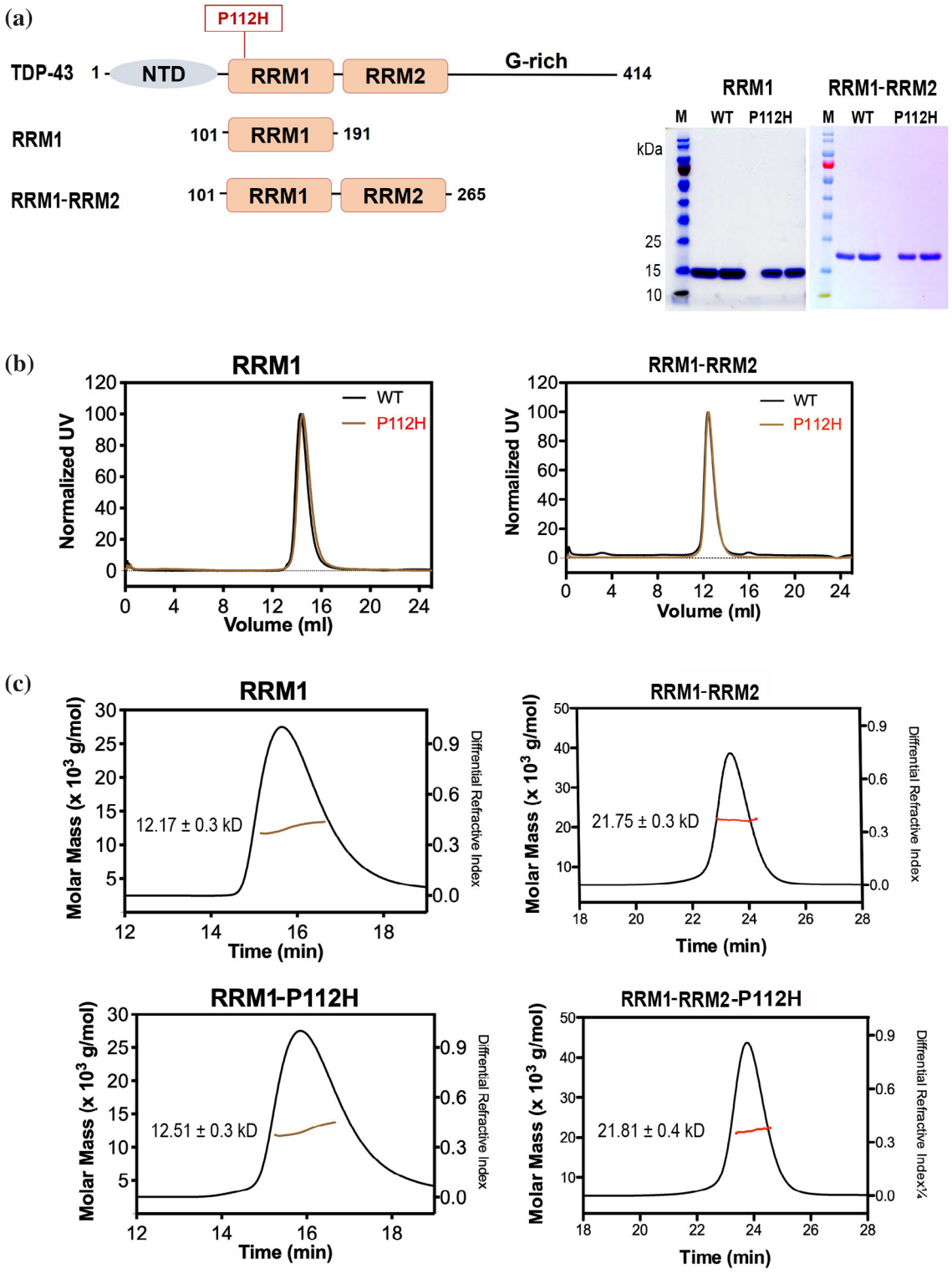

FIGURE 1 TDP-43 P112H mutants exhibit similar oligomeric states to wild-type proteins. (a) The domain organization of full-length TDP-43, and the two truncated proteins, RRM1 and RRM1-RRM2. The SDS-PAGE (right panel) reveals that recombinant RRM1 and RRM1-RRM2 proteins with or without P112H mutation had a high homogeneity. (b) Gel filtration (Superdex 75 10/300 GL column) profiles for the His-tagged recombinant RRM1 and RRM2 with (red) or without P112H (black) mutation. (c) The molar mass of TDP-43 proteins, estimated by size exclusion chromatography-coupled multi-angle light scattering (SEC-MALS): RRM1 (12.17 kD), RRM1-P112H (12.51 kD), RRM1-RRM2 (21.75 kD), and RRM1-RRM2-P112H (21.81 kD). The calculated molecular weights for RRM1 and RRM1-RRM2 are 12.4 and 20.8 kD, respectively

TDP-43 inclusions have commonly been identified in the degenerating neurons of patients with a diverse set of neurodegenerative diseases, including all cases of amyotrophic lateral sclerosis (ALS) and about half of the cases of frontotemporal dementia (FTD) and Alzheimer's disease.[13–15]

ALS is the most prevalent neurodegenerative motor neuron disease (MND), which is characterized by progressive loss of upper and lower motor neurons, ultimately leading to paralysis and respiratory failure.[16] FTD is a heterogeneous neurodegenerative disorder associated with behavioral, cognitive, and linguistic dysfunctions arising from loss of neurons in the frontal and temporal lobes of the brain.[17] Interestingly, overlapping clinical and pathological features of FTD and ALS are frequently observed, with some ALS patients developing cognitive and behavioral impairments, and some FTD patients presenting motor neuron dysfunctions.[18] The clinical syndromes patients display may range from pure ALS without any cognitive or behavioral deficits to pure FTD without MND, or encompass a mix of cognitive/behavioral impairments with MND,[19,20] indicating an unknown but partially shared pathological link between these diseases.

Apart from forming similar TDP-43-positive inclusions, both ALS and FTD patients can exhibit TDP-43 mutations. Although the majority of ALS cases (~90%) are sporadic and of unknown cause, ~3% have been linked to mutations of the TDP-43 encoding gene *TARDBP*.[21] In contrast, ~40% of FTD patients have a family history of the disease,[22,23] with mutations in the *progranulin* (*GRN*) and *microtubule-associated protein tau* (*MAPT*) genes, and hexanucleotide GGGGCC repeat expansion in the chromosome 9 open reading frame 72 (C9orf72) being common.[24] Rare genetic mutations have also been identified in *TARDBP* of FTD patients,[22,24,25] but cases of FTD-associated TDP-43 mutations, that is, without MND, are rare.[26–28] To date, ~60 TDP-43 mutations have been identified from ALS patients, whereas only a few TDP-43 mutations—including A382T, G295S, N267S, K263E, M359V, and I383V—have been reported from FTD patients with or without MND.[24,29] Notably, most ALS/FTD-linked mutations are located in the G-rich region of TDP-43, with only a few exceptions, such as A90V in the NTD, and D169G, K181E and N259S within or adjacent to RRM.[29–31]

Relative to the aforementioned variants, the P112H mutation of TDP-43 is quite unique as it was identified from patients presenting with pure FTD without MND and it is located in RRM1 of TDP-43.[32] This P112H mutation is deemed pathogenic based on clinical, neuroimaging, and neuropathological characteristics of patients possessing it and that present with an unclassified TDP-43 inclusion pattern, a high burden of tau-negative β-amyloid neuritic plaques, and an unclassifiable four-repeat tauopathy.[32] The co-occurrence of multiple protein inclusions is indicative of a pathogenic mechanism that promotes protein interaction and/or aggregation, or that loss of TDP-43 function somehow impairs protein clearance. Thus, to clarify the molecular mechanism underlying the pathogenic effect of P112H mutation, it is necessary to examine its impact on TDP-43 at the protein level.

Here, we compare the biochemical and biophysical properties of two truncated TDP-43 proteins, RRM1 (residues 101–191) and RRM1-RRM2 (residues 101–265), bearing the P112H mutation with those of wild-type proteins. We show that P112H mutation of TDP-43 RRMs induces local protein conformational changes and increases protein thermal stability yet reduces both RNA-binding activity and protein aggregation ability. Our 2D-nuclear-magnetic resonance (NMR) spectrometry analysis confirms those local conformational changes surrounding the P112H mutational site. Together, our results reveal that P112H mutation of TDP-43 may impair the protein's function in RNA metabolism and curtail protein clearance.

2 | RESULTS

2.1 | TDP-43 P112H mutant proteins retain overall folding and oligomeric states of wild-type protein

To examine the impact of disease-linked P112H mutation on TDP-43, we expressed and purified two truncated forms of TDP-43 protein, with or without P112H mutation; namely, RRM1 and RRM1-P112H (residues 101–191), and RRM1-RRM2 and RRM1-RRM2-P112H (residues 101–265) (Figure 1). Both wild-type and mutated TDP-43 proteins were purified to high homogeneity by chromatographic methods, as shown by SDS-PAGE (Figure 1a, right panel). Gel filtration profiles of wild-type RRM1 and RRM1-RRM2 overlapped with those of RRM1-P112H and RRM1-RRM2-P112H, respectively (Figure 1b), indicating that the P112H mutation did not affect overall protein folding or oligomeric states. Size exclusion chromatography-coupled multi-angle light scattering (SEC-MALS) revealed that wild-type RRM1 and RRM1-RRM2 and mutant RRM1-P112H and RRM1-RRM2-P112H are all monomeric, with estimated molecular weights (MWs) of ~12 kDa (calculated MW: 12,396 Da) and ~22 kDa (calculated MW: 20,794 Da) for wild-type RRM1 and wild-type RRM1-RRM2, respectively (Figure 1c). These results indicate that mutation of Pro112 to His in RRM1 does not affect the overall folding and oligomeric state of TDP-43.

2.2 | P112H mutation in TDP-43 increases protein thermal stability

To examine the effect of P112H mutation on protein thermal stability, we performed differential scanning fluorimetry (DSF) using SYPRO Orange dye as the fluorophore to measure the thermal melting points of wild-type and mutated proteins. We found that RRM1-P112H had a melting point of 67.3 ± 0.2°C, which was 3.3°C higher than the melting point (64.0 ± 0.3°C) of the wild-type RRM1 (Figure 2a). RRM1-RRM2-P112H also exhibited a similar trend in that its melting point (57.8 ± 0.3°C) was 4.3°C higher than the melting point of 53.5 ± 0.5°C for wild-type RRM1-RRM2.

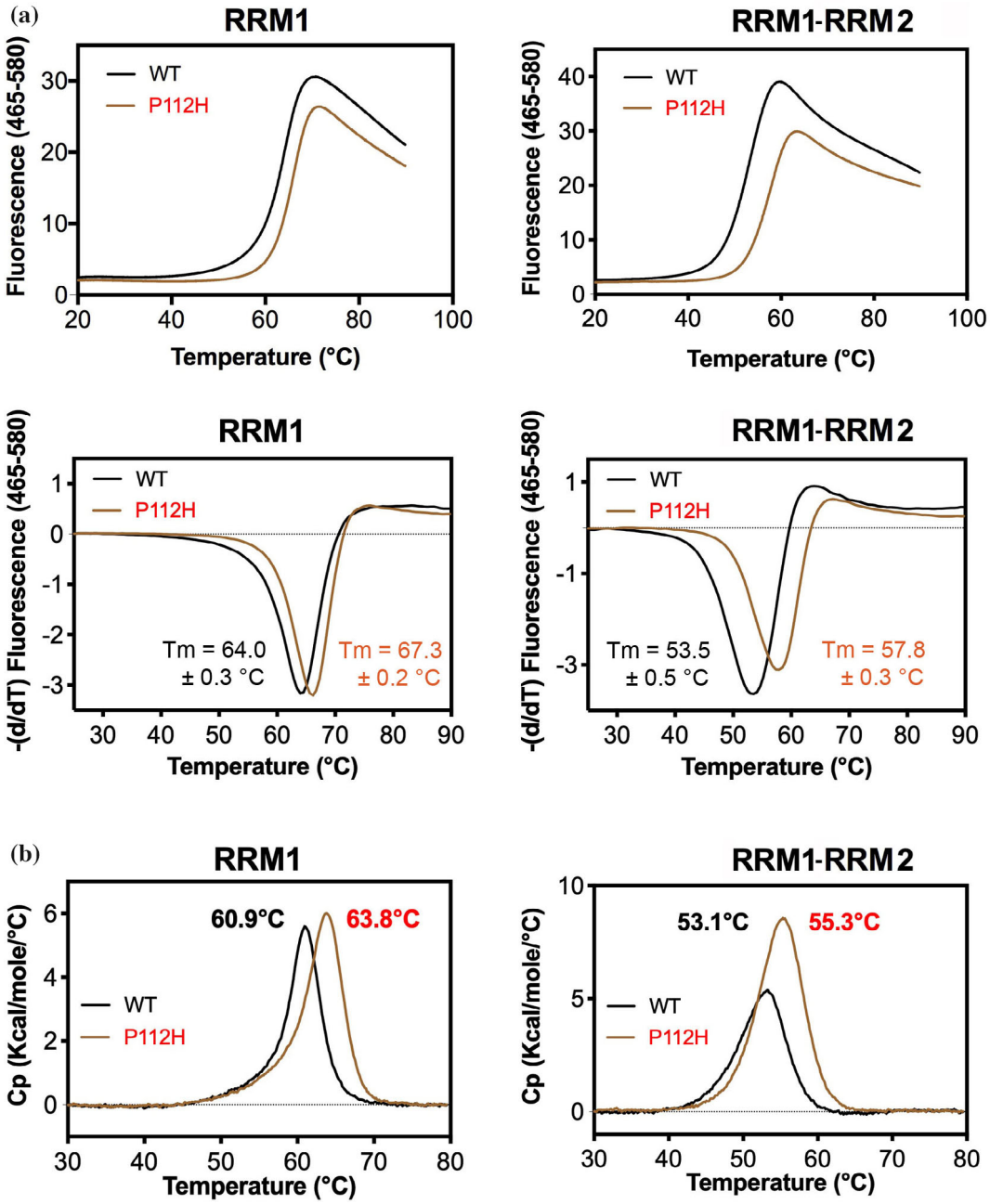

FIGURE 2 Mutation of P112H in TDP-43 increases protein thermal stability. (a) The thermal melting points of wild-type (in black) and P112H-mutated (in red) TDP-43 were assayed by differential scanning fluorimetry using SYPRO Orange dye as the fluorophore. The fluorescence signal, excited at 465 nm and emitted at 580 nm, was recorded while increasing the temperature from 20 to 90°C (upper panels). The melting point of each protein was estimated based on the derivatives of the fluorescence signal against temperature (shown in the lower panels and reflecting three independent measurements). (b) The thermal melting points of wild-type TDP-43 (in black) and P112H mutants (in red) were estimated by differential scanning calorimetry

To further confirm these results, the thermal melting points of these wild-type and mutated proteins were also measured by differential scanning calorimetry (DSC). The DSC-measured melting points were a few degrees lower than those estimated by DSF, but the results were consistent in that RRM1-P112H had a melting point 2.9°C higher than that of wild-type RRM1 (60.9°C), whereas RRM1-RRM2-P112H had a melting point 2.2°C greater than that of wild-type RRM1-RRM2 (53.1°C) (Figure 2b). Thus, all these results reveal that P112H mutation significantly increases the thermal stability of TDP-43, hinting that the mutation may disturb the process of cellular protein clearance.

2.3 | P112H mutation induces tertiary conformational changes in TDP-43 RRM1

To characterize if the disease mutation P112H affects protein secondary structure, we analyzed wild-type and mutated TDP-43 proteins by far-UV (190–260 nm) circular dichroism (CD). Wild-type RRM1 and RRM1-P112H presented similar far-UV CD spectra, suggesting that the P112H mutation did not induce major protein structural changes at the secondary structure level (Figure 3a). Similarly, the far-UV CD spectra of wild-type RRM1-RRM2 and RRM1-RRM2-P112H overlapped considerably, supporting that RRM1-RRM2-P112H retained a secondary structure similar to that of wild-type protein (Figure 3a).

To examine tertiary structural change of TDP-43 upon P112H mutation, we compared the near-UV (260–350 nm) CD spectra of wild-type and mutated TDP-43 proteins. The CD spectrum in the near-UV region (260–320 nm) reflects the environments of aromatic amino acids and may provide a valuable fingerprint of protein tertiary structure.[33] Particularly, Pro112 is located right next to Trp113, which has a peak between 290 to 305 nm in near-UV CD (see Figure 3b for the peak region of Phe, Tyr, and Trp). The side chain of Trp113 is highly exposed on TDP-43 surface, responsible for interactions with nucleic acids.[34] Mutation of Pro112 to His may disturb the conformation or environment of Trp113 that could be detected by near-UV CD. However, the near-UV signals were very weak, so we had to increase the protein concentration (from 10 μM for far-UV CD) to ∼160 μM using a big cuvette with a 10 mm path length to strongly enhance the near-UV CD signals. Significant changes around 290 nm were observed in the near-UV CD spectrum of RRM1-P112H relative to respective wild-type RRM1, suggesting that the P112H mutation induced tertiary structural conformational changes (Figure 3b). A similar outcome was observed for the near-UV CD spectra of RRM1-RRM2 and RRM1-RRM2-P112H proteins with considerable changes in 260–320 nm (Figure 3b). These changes in the near-UV CD support the notion that P112H mutation produces tertiary conformational changes in TDP-43.

To confirm that these structural changes are indeed caused by the P112H mutation, we also expressed and purified two additional TDP-43 RRM1 mutants, that is, RRM1-D169G and the double mutant RRM1-P112H-D169G. Near-UV CD spectra of these mutant proteins revealed almost complete concordance between RRM1-D169G and wild-type RRM1 (Figure 3c), in line with a previous report on crystal structures showing that RRM1-D169G is almost identical to wild-type RRM1.[35] However, the near-UV CD spectrum of the double mutant RRM1-P112H-D169G overlapped well with that of RRM1-P112H, suggesting that the structural change is indeed due to P112H mutation of RRM1. Based on these CD results, we conclude that mutation of P112H induces tertiary conformational changes in RRM1 of TDP-43.

2.4 | TDP-43 P112H mutants are resistant to aggregation

RRMs of TDP-43 and FUS have been shown to self-assemble into Thioflavin-T (ThT)-positive amyloid aggregates in vitro.[36–38] To further establish the mechanism underlying pathogenicity of the P112H mutation in TDP-43, we assayed the amyloid aggregation formation activity of wild-type and mutated TDP-43 proteins. As anticipated, we found that wild-type RRM1 and RRM1-RRM2 self-assembled into ThT-positive amyloid aggregates upon agitation in a buffer of 25 mM Tris–HCl and 100 mM NaCl (Figure 4a). In contrast, RRM1-P112H did not form ThT-positive aggregates under the same conditions, whereas RRM1-RRM2-P112H formed much less than those generated by wild-type proteins.

It has been reported previously that, under oxidative stress, TDP-43 undergoes abnormal disulfide cross-linking and oligomerization via cysteine oxidation.[39] Cysteine residues (Cys173 and Cys175) in the RRM1 domain of TDP-43 contribute to oligomerization and pathogenicity of TDP-43.[40] Moreover, previous study has shown that TDP-43 constructs containing the RRM1 domain undergo an oxidation-induced conformational change, rendering them susceptible to irreversible aggregation upon oxidation.[41] To test if the disease-linked P112H mutation, which is located in close proximity to Cys173, exerts any effect on TDP-43 oxidation, we analyzed protein aggregation after H_2O_2 treatment by turbidity assays. Consistent with previous reports, we found that oxidation of wild-type RRM1 and RRM1-RRM2 by H_2O_2 (5 mM) induced

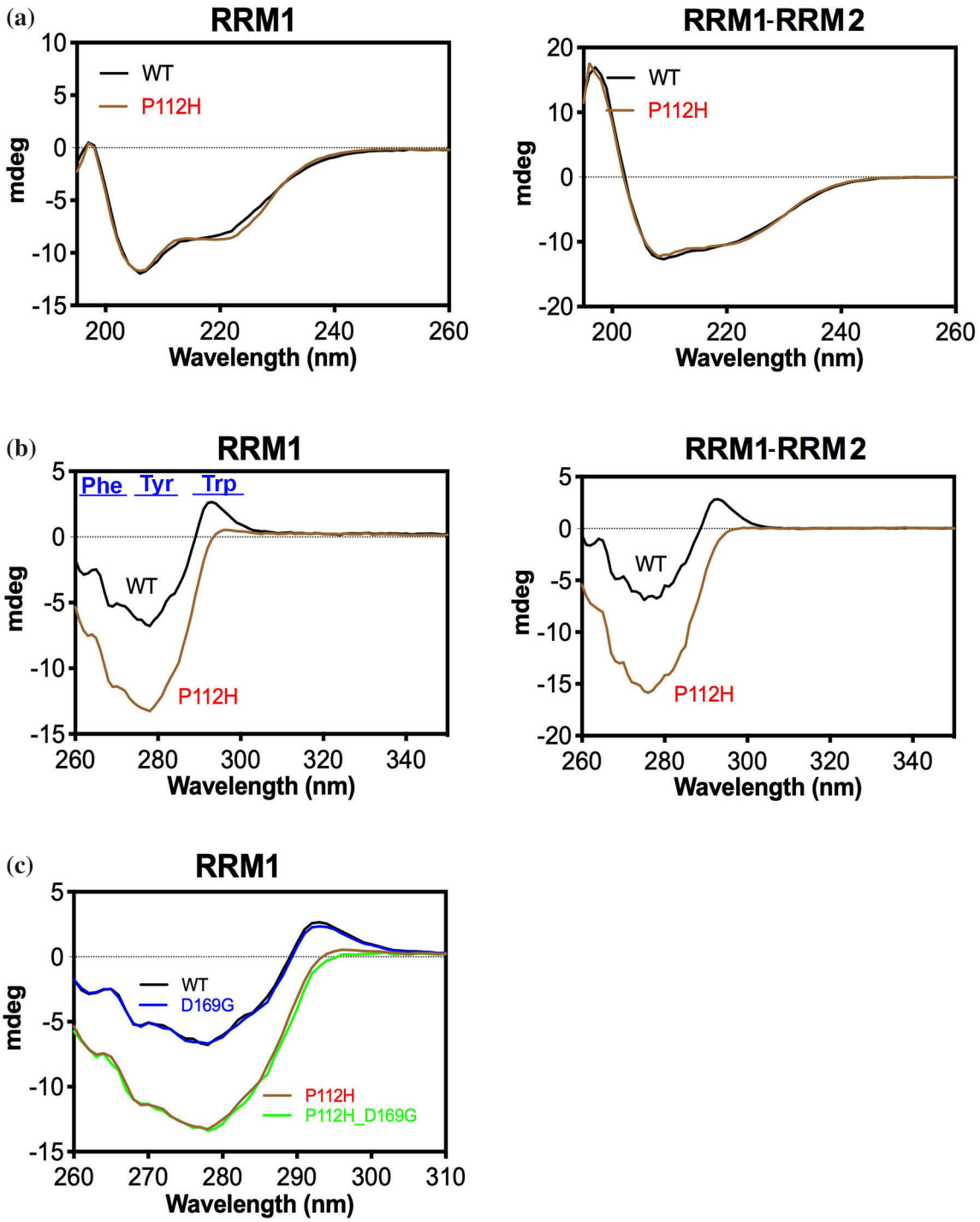

FIGURE 3 Circular dichroism (CD) reveals conformational changes induced by P112H mutation in TDP-43. (a) The far-UV CD spectra of wild-type TDP-43 proteins (in black) and P112H mutants (in red) were recorded from 190 to 260 nm at 25°C at a protein concentration of 10 μM in a buffer containing 10 mM phosphate (pH 7.5) in a quartz cell with 1-mm path length. (b) The near-UV CD signal (from 260 to 350 nm) for each protein was recorded at a high protein concentration of 2 mg/ml in PBS buffer at 25°C in a quartz cuvette with 10-mm path length. The peak region (260–310 nm) arise from aromatic amino acids are marked in the near-UV CD of RRM1. (c) The near-UV CD spectra for RRM1, RRM1-P112H, RRM1-D169G, and RRM1-P112H-D169G. Significant changes were observed in the spectra of RRM1-P112H (in red) and RRM1-P112H-D169G (green), but not in RRM1-D169G (blue), relative to that of wild-type RRM1 (black)

protein aggregation (Figure 4b). However, protein aggregation upon oxidation of the RRM1-P112H and RRM1-RRM2-P112H mutants was significantly reduced compared to wild-type proteins. Thus, the resistance of P112H mutants to oxidation-induced aggregation might be related to mutation-associated conformational changes close to

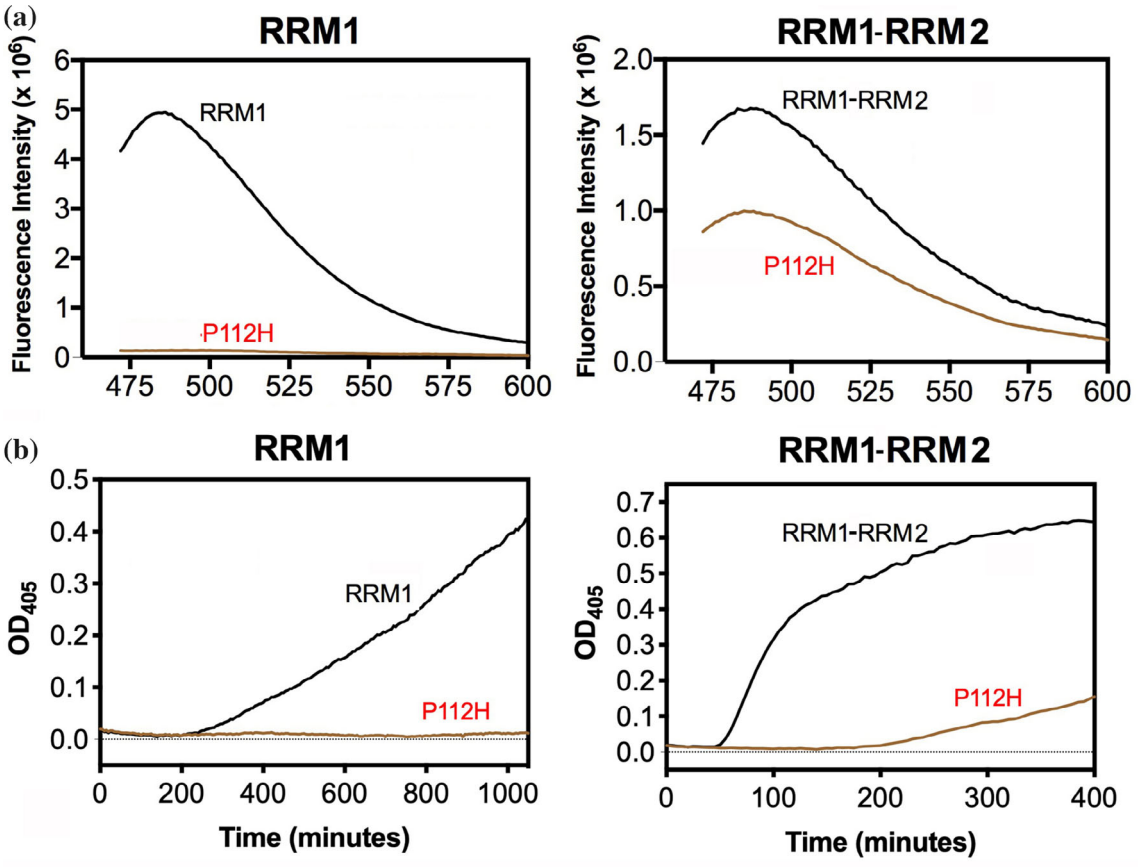

FIGURE 4 TDP-43 P112H mutants are resistant to forming amyloid inclusions and oxidation-induced aggregation. (a) Time-course experiments showing that TDP-43 RRM1 and RRM1-RRM2 formed amyloid inclusions in Thioflavin-T (ThT) binding assays upon agitation in a buffer containing 25 mM Tris–HCl (pH 8.0 for RRM1 or pH 9.0 for RRM1-RRM2) and 100 mM NaCl. In contrast, RRM1-P112H and RRM1-RRM2-P112H were resistant to formation of ThT-positive inclusions under the same conditions. (b) TDP-43 RRM1 and RRM1-RRM2 formed oxidation-induced aggregates upon treatment with 5 mM H_2O_2, as revealed by the turbidity assay, whereas RRM1-P112H and RRM1-RRM2-P112H formed significantly less oxidation-induced aggregates under the same conditions

residue Cys173, which likely becomes inaccessible to disulfide cross-linked bond formation. Together, these results show that P112H-mutated TDP-43 proteins are less prone to aggregation under oxidizing or non-oxidizing conditions.

2.5 | TDP-43 P112H mutants have reduced RNA-binding activities

RRM1 in TDP-43 is involved in RNA binding, and loss of RNA-related functions could contribute to pathogenicity and disease onset,[1,42] so we wondered if the P112H mutation impairs the RNA-binding activity of TDP-43. Consequently, we measured the RNA-binding affinity of our truncated RRM1 and RRM1-RRM2 proteins for a single-stranded 12-nucleotide (nt) 5′-fluorophore (FAM)-labeled $(UG)_6$ RNA by fluorescence polarization assays. We found that the RNA-binding affinity of RRM1-P112H was three-fold lower (Kd = 148.7 ± 3.4 nM) than that of wild-type RRM1 (Kd = 56.9 ± 2.1 nM), and the RNA-binding affinity of the RRM1-RRM2-P112H mutant (Kd = 71.6 ± 2.9 nM) was about eight-fold lower than that of wild-type RRM1-RRM2 (Kd = 9.5 ± 1.3 nM) (Figure 5). Thus, the disease-linked P112H mutation reduces the RNA-binding activity of TDP-43 and, accordingly, may impair its various cellular functions in RNA metabolism.

The P112H mutation is located in Loop1 between the β1 strand and α1 helix of RRM1 (Figure 6a). A crystal structure of TDP-43 RRM1-DNA complex revealed that the Trp113 side chain located in Loop1 is sandwiched between two nucleobases, making π-π stacking interactions with the single-stranded DNA (ssDNA) (Figure 6a).[43] Mutation of Trp113 to Ala (W113A) considerably reduced the interaction of RRM1 with a 30-nt ssDNA (Kd = 114.5 nM for W113A mutant vs. Kd = 20.6 nM for wild-type RRM1).[43,44] Mutation of P112H likely alters the side chain conformation of the neighboring Trp113, thereby reducing the

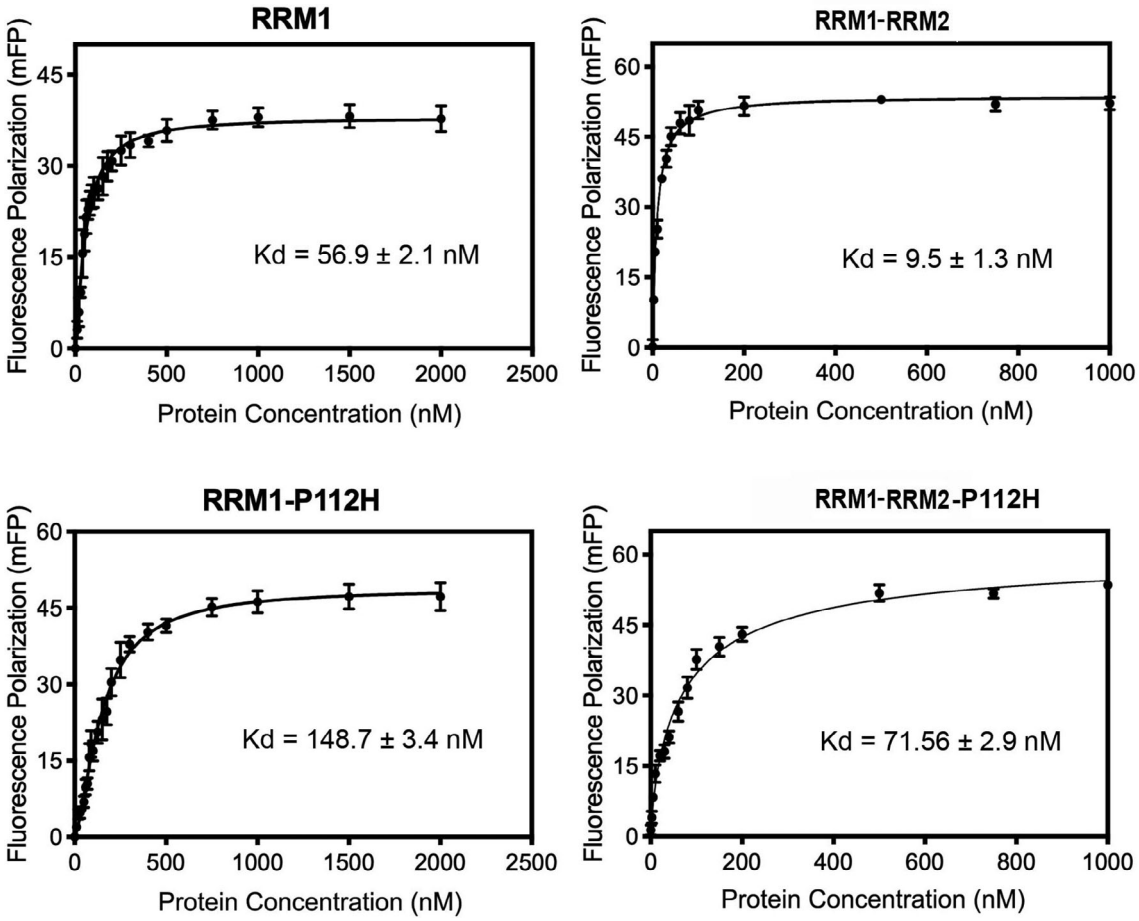

FIGURE 5 P112H mutation of TDP-43 reduces RNA-binding activity. The RNA-binding affinities of TDP-43 RRM1 and RRM1-RRM2 proteins with or without P112H mutation for a 5′-end FAM-labeled $(UG)_6$ RNA were measured by fluorescence polarization assays. The dissociation constants (Kd) and standard deviations shown in the figure were estimated from three independent measurements

mutant protein's binding affinity for ssRNA. To confirm that hypothesis, we measured the intrinsic protein fluorescence of RRM1 and RRM1-RRM2, as previous study showed that intrinsic fluorescence signal of RRM1 was reduced upon ssDNA binding due to local environmental changes surrounding Trp113.[45] We used two different ssDNA substrates for this assay, that is, 10-nt (10TG_DNA) and 12-nt (12ATG_DNA) ssDNAs that were used in previous crystal structural and NMR structural analyses, respectively.[43,46] As reported previously, we observed diminished fluorescence signal for wild-type RRM1 and RRM1-RRM2 in the presence of ssDNA when the temperature was lower than the proteins' melting point (~65°C), indicative of local environmental changes surrounding Trp113 upon ssDNA binding to the folded protein (Figure 6b). In contrast, no change was observed in the fluorescence signal for RRM1-P112H or RRM1-RRM2-P112H upon DNA binding when proteins were folded or unfolded, demonstrating that Trp113 of P112H mutants is not involved in DNA interactions (Figure 6b). These results suggest that mutation of Pro112 to His in TDP-43 reduces the protein's RNA-binding activity, likely due to disruption of interactions between Trp113 and RNA.

2.6 | P112H mutation perturbs RRM1 conformation

To determine the molecular basis for the reduced RNA-binding activity of TDP-43 P112H mutants, we conducted NMR spectrometry on wild-type and mutated RRM1 to detect if the mutation induces any conformational changes. We prepared ^{15}N-labeled wild-type RRM1 and RRM1-P112H, and acquired 2D ^{15}N/^{1}H HSQC spectra for these two proteins. The peak assignment for the 2D ^{15}N/^{1}H HSQC spectrum of wild-type RRM1 was imported from BMRB entry 18,765.[41] An overlay of the wild-type RRM1 ^{15}N-HSQC spectrum (Figure 7a, red) with that of the RRM1-P112H spectrum (blue) showed that the P112H mutation induced significant structural changes, with ~20% of the RRM1-P112H peaks not matching the respective ones of wild-type RRM1 (a plot of chemical

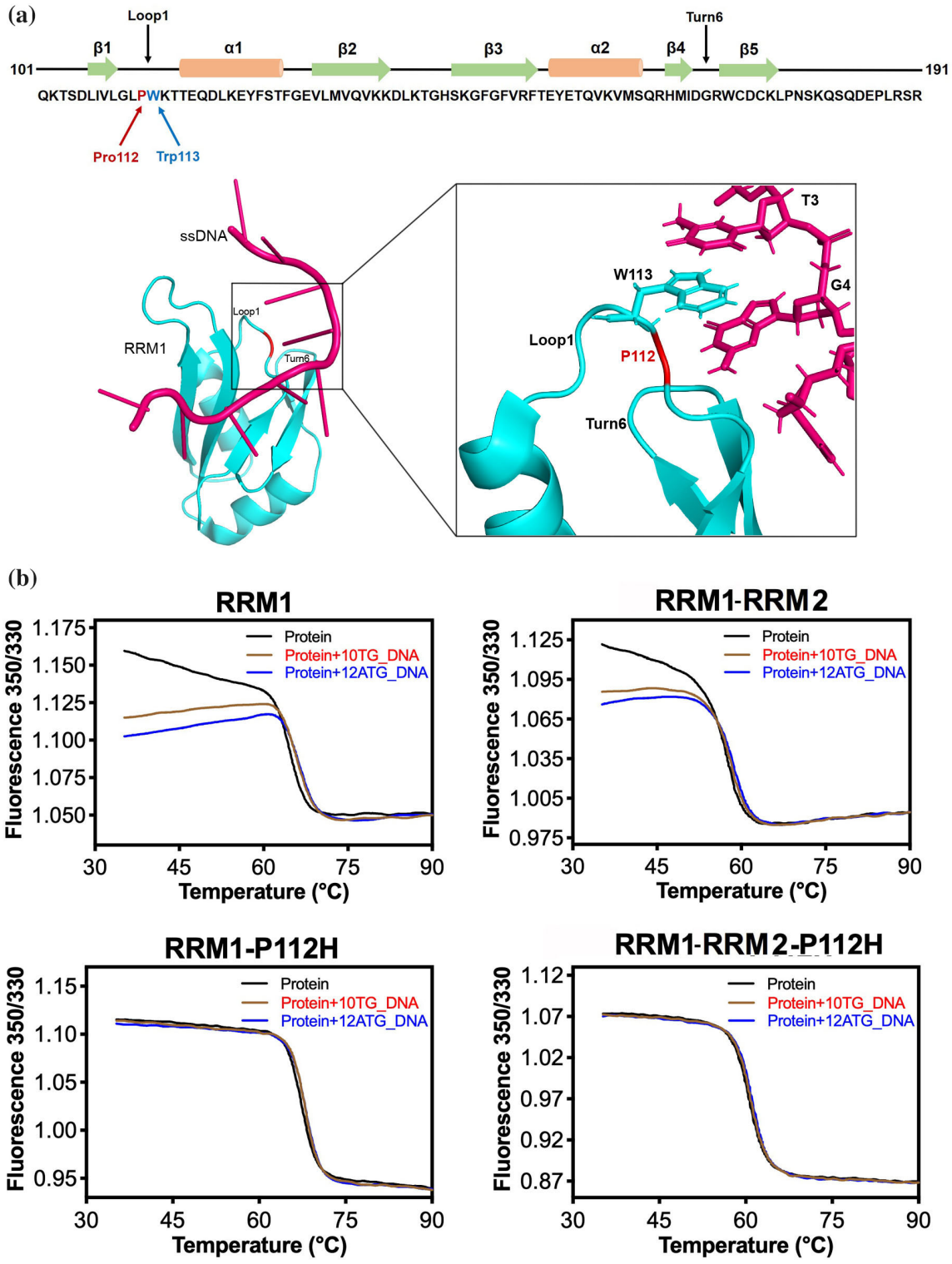

FIGURE 6 P112H mutation of TDP-43 RRM1 disrupts the interactions between Trp113 and nucleic acids. (a) The P112H mutation is located in Loop1 of RRM1. The crystal structure of TDP-43 RRM1-DNA complex (PDB entry: 4IUF) shows that the side chain of Trp113 is sandwiched between two nucleobases, making π-π stacking interactions with DNA.[43] (b) Intrinsic tryptophan fluorescence profiles (ratio of absorption at 350/330 nm) of wild-type RRM1 and RRM1-RRM2 reveal diminished signal upon binding of a 10-nt (10TG_DNA) or 12-nt (12ATG_DNA) DNA (upper panels). However, RRM1-P112H and RRM1-RRM2-P112H presented similar intrinsic tryptophan fluorescence profiles (lower panels) in the presence or absence of DNA, indicating that the environment surrounding residue Trp113 was not changed upon DNA binding

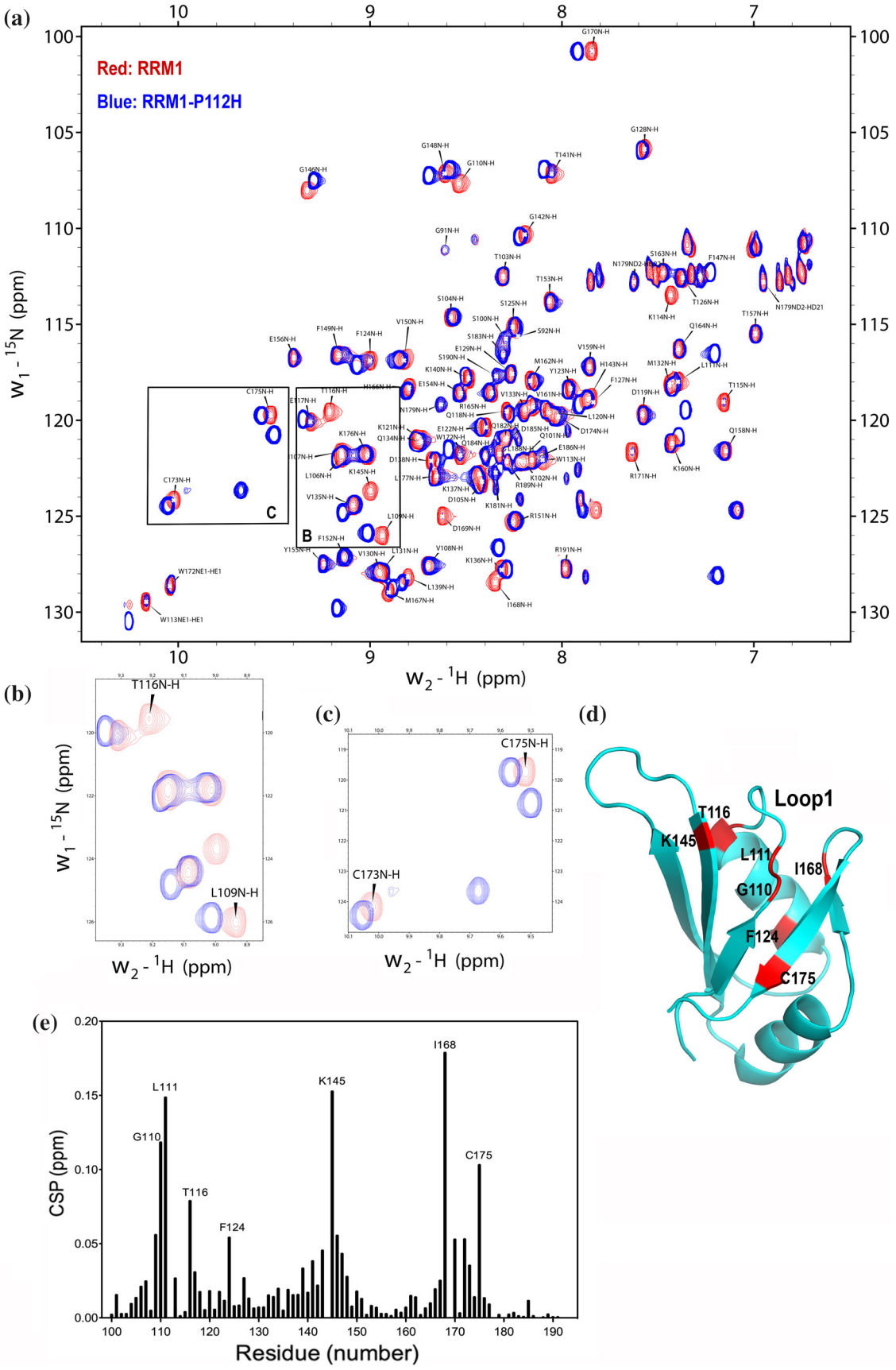

FIGURE 7 Legend on next page.

shift perturbation [CSP] for each residue is shown in Figure 7e). It should be noted that these HSQC peak shifts might be due to the changes in protein dynamics and/or surrounding chemical environments, other than resulted from structural changes. We mapped the amino acids of the RRM1-P112H mutant exhibiting significant HSQC peak shifts onto the available crystal structure of TDP-43 RRM1 (shown in red in Figure 7d), most of which resided in Loop1 (residues 109–116). A representative closer examination of residues Leu109 and Thr116 (both N-H atoms) exemplifies the strong perturbations within Loop1 (Figure 7b). These results confirm that the P112H mutation induces local conformational changes surrounding the mutational site.

Moreover, we also observed perturbations around Cys173 and Cys175 in RRM1-P112H (Figure 7c), suggesting structural changes at these Cys residues. These results are in agreement with our finding that the RRM1-P112H and RRM1-RRM2-P112H mutants are more resistant to oxidation and subsequent aggregation. These NMR spectra reveal that the mutation of Pro112 to His in Loop1 results in local conformational changes, particularly at Loop1 and Turn6, offering a plausible explanation for the altered biochemical and biophysical properties of the TDP-43 P112H mutants, including their higher thermal stability, greater resistance to protein aggregation, and reduced RNA-binding activity.

3 | DISCUSSION

In this study, we have compared the biochemical and biophysical properties of disease-linked TDP-43 P112H mutants to wild-type proteins. We observed unexpectedly that RRM1-P112H and RRM1-RRM2-P112H mutant proteins exhibit significantly greater thermal stability than wild-type proteins. Proline is a unique amino acid with a side chain bonded to the backbone nitrogen, forming a five-membered pyrrolidine ring. This ring conformation restricts the rotation of the N–Cα bond, and decreases the backbone conformational entropy, that may enhance protein stability upon protein folding.[47] Various examples have shown that replacement of different amino acids to proline decreases the entropy of folding and thus increases protein thermal stability.[48,49] On the contrary, proline is also a secondary structure breaker due to the absence of a hydrogen atom on the amide nitrogen, prohibiting proline from acting as a donor in a hydrogen bond.[50] Mutation of different residues to proline may produce conflicting results of decreasing protein thermal stability.[51] Therefore, replacement of a Pro to His may affect protein thermal stability dependent on the location of the proline residue in the folded protein. Pro112 is located in the middle of Loop1 exposing on the surface of RRM1 in TDP-43, and hence the mutation of Pro112 to His should not produce unfavorable steric clashes for protein folding. We generated a structural model of RRM1-P112H using the crystal structure of wild-type RRM1 as the template, showing that the side chain of His112 (Nδ1 atom) could form a hydrogen bond with the main-chain nitrogen of Trp113 to stabilize Loop1 conformation in RRM1 (Figure 8). This structure model suggests that P112H mutation may decrease the flexibility of Loop1 and thus increase thermal stability of TDP-43.

To our knowledge, P112H mutation in TDP-43 is not the only one with a change of increasing protein thermal stability. The D169G mutation of TDP-43 RRM1 was also shown previously to enhance protein thermal stability and cleavage by caspase 3, resulting in greater accumulation and aggregation of cellular pathogenic protein fragments (TDP-35).[35] Moreover, several ALS-linked mutations of TDP-43—including K263G, G298S, Q331K, and M337V—also induce longer half-lives and greater stability relative to wild-type TDP-43.[52–54] These results indicate that TDP-43 protein stability may be a major contributor to the pathogenesis of ALS and FTD. We also noticed that TDP-43 RRMs harboring the P112H mutation are less prone to forming ThT-positive aggregates and more resistant to oxidation-induced protein aggregation relative to wild-type protein, indicating that P112H mutation reduces the intrinsic propensity of TDP-43 to aggregate. Taken together, these results support the notion that by increasing the protein stability of TDP-43, the P112H mutation might cause defects in cellular protein clearance and thereby contribute to TDP-43 proteinopathy.

FIGURE 7 2D-NMR reveals that the P112H mutation perturbs TDP-43 RRM1 conformation. (a) Superimposition of the ^{15}N-HSQC NMR spectra of wild-type RRM1 (in red) and RRM1-P112H (in blue), revealing that the P112H mutation induces peak shifts. The peak assignments for the wild-type RRM1 spectrum were imported from BMRB entry 18,765. (b) A representative region shows that residues Leu109 and Thr116 located within Loop1 of RRM1-P112H exhibit significant shifts of HSQC peaks. (c) A closer look at the HSQC spectrum highlights the peak shifts in two cysteine residues of RRM1-P112H. (d) Amino acids exhibiting significant shifts of HSQC peaks (marked in red) occur mainly in two regions, Loop1 and Turn6, and are mapped onto the RRM1 structure. (e) The chemical shift perturbation (CSP) between the ^{15}N-HSQC spectra of RRM1 and RRM1-P112H were calculated and plotted as a function of residue number. No value is shown for residues that could not be assigned in one or both spectra

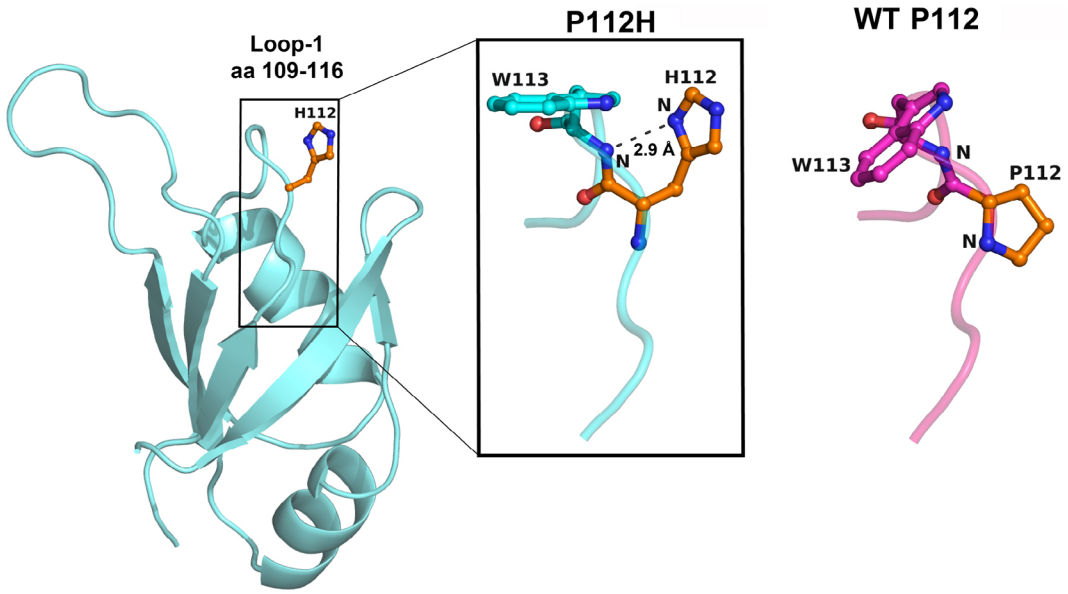

FIGURE 8 Molecular model of TDP-43 RRM1-P112H mutant. The molecular model of RRM1-P112H was built using the crystal structure of wild-type RRM1 (PDB entry: 4Y0F) as the template.[43] The geometry of the initial RRM1-P112H model was optimized using the modeling tool in PHENIX (version 1.13–2,298). In the final model, the side chain (Nδ1 atom) of His112 located in Loop1 forms a hydrogen bond with the main-chain nitrogen of Trp113, suggesting that P112H mutation likely decreases the loop flexibility, and thus increases the thermal stability of TDP-43

Loss-of-function in RNA binding and impairment in RNA metabolism of TDP-43 could also contribute to disease pathogenesis. We show through near-UV CD and 2D-NMR spectrometry that the P112H mutation induces local structural changes in RRM1 of TDP-43 surrounding the mutation site, particularly in Loop1 and Turn6. These conformational changes disrupt the π-π stacking interaction between Trp113 and RNA, so TDP-43 P112H mutants bind RNA with a lower affinity relative to wild-type proteins. Some TDP-43 mutations compromise the protein's splicing ability for specific mRNA transcripts. For instance, alternative splicing of the *POLDIP3* gene depends on RRM1, and P112H-mutated TDP-43 is deficient in restoring normal *POLDIP3* splicing in TDP-43 knockout cell lines.[55,56] A similar result has been reported for the ALS/FTD-linked TDP-43 K181E mutation, with that residue being located in close proximity to RRM1. TDP-43 K181E mutant protein completely lacks the ability to interact with a 12-nt RNA in vitro and fails to splice out exon 3 of *POLDIP3*.[31] However, unlike the P112H mutation, K181E-mutated TDP-43 is prone to aggregation and forms abundant aggregates in transfected cells,[31] suggesting that although both these mutations occur in or near RRM1, they induce mechanistically divergent outcomes at protein level and can be linked to different disease phenotypes (i.e., pure FTD for P112H mutation, and ALS/FTD for K181E mutation). Our results show that the P112H mutation of TDP-43 impairs its RNA binding function, causing RNA splicing defects and/or other dysfunctions in RNA metabolism.

In conclusion, our findings reveal that the P112H single-site mutation of TDP-43 induces local conformational changes in RRM1, leading to increased protein stability and impaired RNA binding, as well as a reduced tendency to aggregate. Our analyses reveal potential molecular links between TDP-43 P112H mutation and FTD pathogenesis, including a loss-of-function in RNA binding that could contribute to impaired RNA metabolism and a gain-of-function in increased protein stability that could induce defects in cellular protein clearance.

4 | MATERIALS AND METHODS

4.1 | Site-directed mutagenesis, protein expression, and purification

The cDNA encoding wild-type RRM1 (residues 101–191) and RRM1-RRM2 (residues 101–265) were amplified from the human *TARDBP* gene and inserted into the BamHI/HindIII sites of pQE30 vector (Qiagen) for expression of the N-terminal His-tagged recombinant proteins. TDP-43 mutants—RRM1-P112H, RRM1-D169G, RRM1-RRM2-P112H and RRM1-P112H-D169G—were generated by site-directed mutagenesis using a QuikChange site-directed mutagenesis kit (Stratagene) with wild-type plasmids as templates. TDP-43 expression plasmids were transformed into *Escherichia coli* M15 strain and grown by cell culture at 37°C in LB medium supplemented with 100 μg/ml

ampicillin. When the optical density (OD_{600}) of the cell culture had reached 0.6, it was cooled down to 18°C and induced by adding 0.8 mM isopropyl 1-thio-β-D-galactopyranoside (IPTG), and then cultured for 16–18 hr at 18°C. The cells were harvested by pelleting down the culture and resuspending it in 50 mM phosphate buffer (pH 7.5), 500 mM NaCl, and 10 mM β-mercaptoethanol (βME), together with a tablet of complete EDTA-free protease inhibitor cocktail (Roche). The cells were lysed using a microfluidizer (Microfluidics M-110P) and the cell supernatant was applied to a HisTrap FF column (GE Healthcare), followed by a HiTrap Heparin HP column (GE Healthcare) and finally a HiLoad 16/600 Superdex 75 pg column (GE Healthcare). The purity of the eluted proteins was checked by 12% SDS polyacrylamide gel electrophoresis.

4.2 | Multi-angle light scattering

The molecular mass of wild-type and mutated TDP-43 RRM proteins was measured by SEC-MALS (size exclusion chromatography coupled with multi-angle light scattering). The purified protein samples were centrifuged at 4°C and 13,000 rpm for 30 min and filtered through a 0.22-μm Millex-GV filter (Millipore). The samples were injected into a pre-equilibrated Agilent Bio SEC-3100 Å column (Agilent Technologies, for RRM1) or Superdex 75 10/300 GL column (GE Healthcare, for RRM1-RRM2) connected to a DAWN HELIOS II-18 angle MALS instrument (Wyatt Technology) with a refractive index (RI) detector (Optilab T-rEX, Wyatt Technology). Samples were run using the ÄKTA-UPC 900 FPLC system (GE Healthcare). The UV, scattering and refractive index data were analyzed using ASTRA software (Wyatt Technology) to calculate the molar mass of each sample.

4.3 | Differential scanning fluorimetry

The DSF experiments were carried out using a LightCycler 480 system (Roche). Assay parameters, including dye concentration and protein concentration, were optimized prior to performing the experiments. Samples containing a final protein concentration of 10 μM protein and 15X SYPRO Orange dye (Invitrogen) were used in a LightCycler multi-well 96 white plate (Roche), with a total volume of 20 μL for each sample. The thermal melting point was assessed by raising the temperature from 20 to 90°C at a rate of 0.06°C/s, with 10 acquisitions per degree. An excitation filter of 465 nm and an emission filter of 580 nm were used for SYPRO Orange detection. Melting temperatures (Tm) were calculated by LightCycler® protein melting analysis.

4.4 | Differential scanning calorimetry

An auto PEAQ-DSC Malvern capillary differential scanning calorimeter was used to precisely measure the stability and Tm of wild-type and mutated TDP-43. Protein samples at a concentration of 0.5 mg/ml in 1× PBS were used. The temperature was increased from 10 to 90°C at a scanning rate of 240°C/hr in high feedback mode. For each sample, a blank buffer scan was used for buffer subtraction. The raw data were processed and a Tm report was generated in MicroCal PEAQ-DSC software (Malvern).

4.5 | CD spectroscopy

A Chirascan-plus CD spectrometer (Applied Photophysics) was used to record the near-UV and far-UV CD signal for each protein sample. To assess secondary structure, far-UV CD spectra were scanned from 190 to 260 nm at 25°C. For far-UV CD, protein samples at a concentration of 10 μM in a buffer containing 10 mM phosphate (pH 7.5) were measured in a quartz cell with 1-mm path length. Near-UV CD signal (from 260 nm to 350 nm) for each protein was recorded at a high concentration of 2 mg/ml in 1× PBS buffer at 25°C in a quartz cuvette of 10 mm path length.

4.6 | In vitro fibrillation and ThT binding assays

Purified protein (50 μM) in a buffer of 25 mM Tris–HCl (pH 8.0 for RRM1 or pH 9.0 for RRM1-RRM2) and 100 mM NaCl was centrifuged at 20,000g for 10 min and filtered through a 0.22-μm Millex-GV filter to remove any insoluble material or aggregates. The samples were then shaken at 200 rpm at 37°C for 3 days to promote fibril formation. The freshly-formed fibrillar solutions (5 μL) were subjected to ThT-binding assays. ThT amyloid binding dye (ThT, purchased from Sigma) was dissolved in water to make a stock solution of 1 mM, which was filtered through a 0.2-μm Sartorius Minisart syringe filter and stored in 1 ml aliquots at −20°C and protected from light. The fibrillar solutions were mixed with ThT dye to a final concentration of 20 μM dye and ~10 μM protein. After 5-min incubation in the dark, the

samples were excited at 438 nm and the fluorescence emission intensity was recorded from 472 to 600 nm on a SpectraMax Paradigm microplate reader (Molecular Devices).

4.7 | Protein aggregation by turbidity measurements

Wild-type or mutated protein samples at a concentration of 1 mg/ml (for RRM1) or 0.5 mg/ml (for RRM1-RRM2) in 1× PBS were treated with 5 mM H_2O_2 or PBS (as a control). Oxidation-induced protein aggregation was measured according to increased sample turbidity by recording light absorbance at 405 nm at room temperature. The optical density at 405 nm for wild-type and mutated proteins was plotted against time to monitor protein aggregation over time upon oxidation.

4.8 | RNA-binding by fluorescence polarization assays

RNA-binding affinity of wild-type and mutated TDP-43 proteins for single stranded $(UG)_6$ RNA was determined by measuring changes in fluorescence polarization (FP) using a Paradigm microplate reader (Molecular Devices) at excitation and emission wavelengths of 485 nm and 538 nm, respectively. The 5′-end fluorescein-labeled single-stranded RNA (sequence 5′-FAM-UGUGUGUGUGUG-3′) at a final concentration of 10 nM was mixed with serially-diluted concentrations of protein in a binding buffer of 20 mM HEPES (pH 7.5), 50 mM NaCl, and 1 mM dithiothreitol (DTT). The samples were prepared in a 384-well OptiPlate-Black (PerkinElmer) and incubated at 37°C for 30 min before obtaining the FP data. FP values were plotted against protein concentration to estimate Kd (dissociation constant) values.

4.9 | Intrinsic fluorescence assay

Wild-type or mutated TDP-43 proteins at 50 μM in 1× PBS were mixed with DNA substrates in a 1:1 M ratio and incubated at room temperature for 30 min. The samples were centrifuged at 20,000 *g* for 5 min to remove any possible precipitants and insolubilities. A NanoTemper Tycho NT.6 system was used to detect fluorescence intensity at 350 nm and 330 nm upon heating the sample from 35 to 95°C with a 30°C/min scanning rate. The fluorescence intensity ratio 350/330 nm versus temperature was plotted to monitor changes in protein-DNA interaction.

4.10 | NMR spectroscopy

The *E. coli* cells harboring the TDP-43 expression vector were grown in M9 minimal medium supplemented with ^{15}N-NH_4Cl (1 g/L). The ^{15}N-labeled proteins were purified in the same way as the un-labeled proteins. The protein samples were prepared in a buffer containing 25 mM HEPES pH 7.0, 125 mM NaCl, and 1 mM DTT. The proteins at a concentration of 0.7 mM in 10% D_2O were centrifuged at 20,000 *g* for 30 min to remove any insolubilities and potential aggregates. The 2D ^{15}N/^{1}H HSQC data were collected using a 600-MHz Bruker Avance spectrometer equipped with a 5-mm TCI CryoProbe at 298 K. The spectra were processed using Topspin 2 (Bruker) and analyzed in NMRFAM Sparky. Backbone assignment for wild-type RRM1 was reported previously (BMRB accession number 18765). The following formula was used to calculate the CSP shown in Figure 7e:

$$\mathrm{CSP} = \sqrt{\frac{(\delta \mathrm{H})^2 + (0.14 \times \delta \mathrm{N})^2}{2}}$$

where δH and δN are the chemical shift changes (in ppm) of ^{1}H and ^{15}N shifts, respectively.

ACKNOWLEDGMENTS

We acknowledge the Biophysics Core Facility and the DNA Sequencing Core Facility (IBMS, AS-CFII-108-115) of the Scientific Instrument Center in Academia Sinica for CD, DSC, and DNA sequencing. We also acknowledge the Biophysics Core of the Institute of Molecular Biology for MALS and fluorescence spectrometry. We thank Ms. Tsun-Ai Yu of the High-Field Nuclear Magnetic Resonance Center (HFNMRC) of Academia Sinica for NMR data acquisition. This work was supported by Academia Sinica and Ministry of Science and Technology, Taiwan.

AUTHOR CONTRIBUTIONS

Sashank Agrawal: Data curation; formal analysis; investigation; writing-original draft. **Monika Jain:** Formal analysis; investigation. **Wei-Zen Yang:** Data curation; formal analysis. **Hanna S. Yuan:** Conceptualization; funding acquisition; project administration; supervision; writing-review and editing.

ORCID

Hanna S. Yuan https://orcid.org/0000-0001-9671-6967

REFERENCES

1. Vanden Broeck L, Callaerts P, Dermaut B. TDP-43-mediated neurodegeneration: Towards a loss-of-function hypothesis? Trends Mol Med. 2014;20:66–71.

2. Sephton CF, Cenik B, Cenik BK, Herz J, Yu G. TDP-43 in central nervous system development and function: Clues to TDP-43-associated neurodegeneration. Biol Chem. 2012;393: 589–594.
3. Butti Z, Patten SA. RNA dysregulation in amyotrophic lateral sclerosis. Front Genet. 2018;9:712.
4. Zhang YJ, Caulfield T, Xu YF, et al. The dual functions of the extreme N-terminus of TDP-43 in regulating its biological activity and inclusion formation. Hum Mol Genet. 2013;22: 3112–3122.
5. Shiina Y, Arima K, Tabunoki H, Satoh J. TDP-43 dimerizes in human cells in culture. Cell Mol Neurobiol. 2010;30:641–652.
6. Janssens J, Van Broeckhoven C. Pathological mechanisms underlying TDP-43 driven neurodegeneration in FTLD-ALS spectrum disorders. Hum Mol Genet. 2013;22:R77–R87.
7. Guenther EL, Cao Q, Trinh H, et al. Atomic structures of TDP-43 LCD segments and insights into reversible or pathogenic aggregation. Nat Struct Mol Biol. 2018;25:463–471.
8. Chen AKH, Lin RYY, Hsieh EZJ, et al. Induction of amyloid fibrils by the C-terminal fragments of TDP-43 in amyotrophic lateral sclerosis. J Am Chem Soc. 2010;132:1186–1187.
9. Jiang LL, Che MX, Zhao J, et al. Structural transformation of the amyloidogenic core region of TDP-43 protein initiates its aggregation and cytoplasmic inclusion. J Biol Chem. 2013;288: 19614–19624.
10. Mompean M, Buratti E, Guarnaccia C, et al. Structural characterization of the minimal segment of TDP-43 competent for aggregation. Arch Biochem Biophys. 2014;545:53–62.
11. Saini A, Chauhan VS. Self-assembling properties of peptides derived from TDP-43 C-terminal fragment. Langmuir. 2014;30: 3845–3856.
12. Saini A, Chauhan VS. Delineation of the core aggregation sequences of TDP-43 C-terminal fragment. Chembiochem. 2011;12:2495–2501.
13. Arai T, Hasegawa M, Akiyama H, et al. TDP-43 is a component of ubiquitin-positive tau-negative inclusions in frontotemporal lobar degeneration and amyotrophic lateral sclerosis. Biochem Biophys Res Commun. 2006;351:602–611.
14. Neumann M, Sampathu DM, Kwong LK, et al. Ubiquitinated TDP-43 in frontotemporal lobar degeneration and amyotrophic lateral sclerosis. Science. 2006;314:130–133.
15. Tan RH, Ke YD, Ittner LM, Halliday GM. ALS/FTLD: Experimental models and reality. Acta Neuropathol. 2017;133: 177–196.
16. Tandan R, Bradley WG. Amyotrophic lateral sclerosis: Part 1. Clinical features, pathology, and ethical issues in management. Ann Neurol. 1985;18:271–280.
17. Mackenzie IR, Neumann M. Molecular neuropathology of frontotemporal dementia: Insights into disease mechanisms from postmortem studies. J Neurochem. 2016;138:54–70.
18. Hu WT, Seelaar H, Josephs KA, et al. Survival profiles of patients with frontotemporal dementia and motor neuron disease. Arch Neurol. 2009;66:1359–1364.
19. Bak TH. Motor neuron disease and frontotemporal dementia: One, two, or three diseases? Ann Indian Acad Neurol. 2010;13: S81–S88.
20. Lillo P, Hodges JR. Frontotemporal dementia and motor neurone disease: overlapping clinic-pathological disorders. J Clin Neurosci. 2009;16:1131–1135.
21. Taylor JP, Brown RH, Cleveland DW. Decoding ALS: From genes to mechanism. Nature. 2016;539:197–206.
22. Pottier C, Ravenscroft TA, Sanchez-Contreras M, Rademakers R. Genetics of FTLD: Overview and what else we can expect from genetic studies. J Neurochem. 2016;138:32–53.
23. Sieben A, Mossevelde SV, Wauters E, et al. Extended FTLD pedigree segregating a Belgian GRN-null mutation: Neuropathological heterogeneity in one family. Alzheimers Res Ther. 2018;10:7.
24. Olszewska DA, Lonergan R, Fallon EM, Lynch T. Genetics of frontotemporal dementia. Curr Neurol Neurosci Rep. 2016; 16:107.
25. Greaves CV, Rohrer JD. An update on genetic frontotemporal dementia. J Neurol. 2019;266:2075–2086.
26. Borroni B, Bonvicini C, Alberici A, et al. Mutation within TARDBP leads to frontotemporal dementia without motor neuron disease. Hum Mutat. 2009;30:E974–E983.
27. Kovacs GG, Murrell JR, Horvath S, et al. TARDBP variation associated with frontotemporal dementia, supranuclear gaze palsy, and chorea. Mov Disord. 2009;24:1843–1847.
28. Borroni B, Archetti S, Del Bo R, et al. TARDBP mutations in frontotemporal lobar degeneration: Frequency, clinical features, and disease course. Rejuvenation Res. 2010;13:509–517.
29. Floris G, Borghero G, Cannas A, et al. Clinical phenotypes and radiological findings in frontotemporal dementia related to TARDBP mutations. J Neurol. 2015;262:375–384.
30. Maurel C, Madji-Hounoum B, Thepault RA, et al. Mutation in the RRM2 domain of TDP-43 in amyotrophic lateral sclerosis with rapid progression associated with ubiquitin positive aggregates in cultured motor neurons. Amyotroph Lateral Scler Frontotemporal Degener. 2018;19:149–151.
31. Chen HJ, Topp SD, Hui HS, et al. RRM adjacent TARDBP mutations disrupt RNA binding and enhance TDP-43 proteinopathy. Brain. 2019;142:3753–3770.
32. Moreno F, Rabinovici GD, Karydas A, et al. A novel mutation P112H in the TARDBP gene associated with frontotemporal lobar degeneration without motor neuron disease and abundant neuritic amyloid plaques. Acta Neuropathol Commun. 2015;3:19.
33. Kelly SM, Jess TJ, Price NC. How to study proteins by circular dichroism. Biochim Biophys Acta. 2005;1751:119–139.
34. Wright GSA, Watanab TF, Amporndana K, et al. Purification and structural characterization of aggregation-prone human TDP-43 involved in neurodegenerative diseases. iScience. 2020; 23:101159.
35. Chiang CH, Grauffel C, Wu LS, et al. Structural analysis of disease-related TDP-43 D169G mutation: Linking enhanced stability and caspase cleavage efficiency to protein accumulation. Sci Rep. 2016;6:21581.
36. Agrawal S, Kuo PH, Chu LY, Golzarroshan B, Jain M, Yuan HS. RNA recognition motifs of disease-linked RNA-binding proteins contribute to amyloid formation. Sci Rep. 2019;9:6171.
37. Zacco E, Martin SR, Thorogate R, Pastore A. The RNA-recognition motifs of TAR DNA-binding protein 43 may play a role in the aberrant self-assembly of the protein. Front Mol Neurosci. 2018;11:372.
38. Lu Y, Lim L, Song J. RRM domain of ALS/FTD-causing FUS characteristic of irreversible unfolding spontaneously selfassembles into amyloid fibrils. Sci Rep. 2017;7:1043.

39. Cohen TJ, Hwang AW, Unger T, Trojanowski JQ, Lee VM. Redox signalling directly regulates TDP-43 via cysteine oxidation and disulphide cross-linking. EMBO J. 2012;31:1241–1252.
40. Shodai A, Morimura T, Ido A, et al. Aberrant assembly of RNA recognition motif 1 links to pathogenic conversion of TAR DNA-binding protein of 43 kDa (TDP-43). J Biol Chem. 2013; 288:14886–14905.
41. Chang CK, Chiang MH, Toh EK, Chang CF, Huang TH. Molecular mechanism of oxidation-induced TDP-43 RRM1 aggregation and loss of function. FEBS Lett. 2013;587:575–582.
42. Weskamp K, Barmada SJ. TDP43 and RNA instability in amyotrophic lateral sclerosis. Brain Res. 2018;1693:67–74.
43. Kuo PH, Chiang CH, Wang YT, Doudeva LG, Yuan HS. The crystal structure of TDP-43 RRM1-DNA complex reveals the specific recognition for UG- and TG-rich nucleic acids. Nucleic Acids Res. 2014;42:4712–4722.
44. Furukawa Y, Suzuki Y, Fukuoka M, et al. A molecular mechanism realizing sequence-specific recognition of nucleic acids by TDP-43. Sci Rep. 2016;6:20576.
45. Li W, Reeb AN, Lin B, et al. Heat shock-induced phosphorylation of TAR DNA-binding protein 43 (TDP-43) by MAPK/ERK kinase regulates TDP-43 function. J Biol Chem. 2017;292: 5089–5100.
46. Lukavsky PJ, Daujotyte D, Tollervey JR, et al. Molecular basis of UG-rich RNA recognition by the human splicing factor TDP-43. Nat Struct Mol Biol. 2013;20:1443–1449.
47. Taler-Vercic A, Hasanbasic S, Berbic S, Stoka V, Turk D, Zerovnik E. Proline residues as switches in conformational changes leading to amyloid fibril formation. Int J Mol Sci. 2017;8:549.
48. Matthews BW, Nicholson H, Becktel WJ. Enhanced protein thermostability from site-directed mutations that decrease the entropy of unfolding. Proc Natl Acad Sci U S A. 1987;84: 6663–6667.
49. Trevino SR, Schaefer S, Scholtz JM, Pace CN. Increasing protein conformational stability by optimizing β-turn sequence. J Mol Biol. 2007;73:211–218.
50. Yang WZ, Ko TP, Corselli L, Johnson RC, Yuan HS. Conversion of a β-strand to an α-helix induced by a single-site mutation observed in the crystal structure of Fis mutant Pro26Ala. Protein Sci. 1998;7:1875–1883.
51. Choi EJ, L Mayo S. Generation and analysis of proline mutants in protein G. Protein Eng Des Sel. 2006;19:285–289.
52. Ling SC, Albuquerque CP, Han JS, et al. ALS-associated mutations in TDP-43 increase its stability and promote TDP-43 complexes with FUS/TLS. Proc Natl Acad Sci U S A. 2010;107: 13318–13323.
53. Watanabe S, Kaneko K, Yamanaka K. Accelerated disease onset with stabilized familial amyotrophic lateral sclerosis (ALS)-linked mutant TDP-43 proteins. J Biol Chem. 2013;288: 3641–3654.
54. Austin JA, Wright GS, Watanabe S, et al. Disease causing mutants of TDP-43 nucleic acid binding domains are resistant to aggregation and have increased stability and half-life. Proc Natl Acad Sci U S A. 2014;111:4309–4314.
55. Fiesel FC, Weber SS, Supper J, Zell A, Kahle PJ. TDP-43 regulates global translational yield by splicing of exon junction complex component SKAR. Nucleic Acids Res. 2012;40: 2668–2682.
56. Roczniak-Ferguson A, Ferguson SM. Pleiotropic requirements for human TDP-43 in the regulation of cell and organelle homeostasis. Life Sci Alli. 2019;2:e201900358.

How to cite this article: Agrawal S, Jain M, Yang W-Z, Yuan HS. Frontotemporal dementia-linked P112H mutation of TDP-43 induces protein structural change and impairs its RNA binding function. *Protein Science*. 2021;30:350–365. https://doi.org/10.1002/pro.3990